



# Deep Co-Training for Semi-Supervised Image Segmentation

Jizong Peng<sup>a,\*</sup>, Guillermo Estrada<sup>b</sup>, Marco Pedersoli<sup>a</sup>, Christian Desrosiers<sup>a</sup>

<sup>a</sup>*ETS Montreal, 1100 Notre-Dame W., Montreal, Canada*

<sup>b</sup>*PUC-Rio, 225 Marquês de São Vicente Street, Rio de Janeiro, Brazil*

---

## Abstract

In this paper, we aim to improve the performance of semantic image segmentation in a semi-supervised setting in which training is effectuated with a reduced set of annotated images and additional non-annotated images. We present a method based on an ensemble of deep segmentation models. Each model is trained on a subset of the annotated data, and uses the non-annotated images to exchange information with the other models, similar to co-training. Even if each model learns on the same non-annotated images, diversity is preserved with the use of adversarial samples. Our results show that this ability to simultaneously train models, which exchange knowledge while preserving diversity, leads to state-of-the-art results on two challenging medical image datasets.

*Keywords:* Deep learning, semi-supervised learning, ensemble learning, co-training, image segmentation

---

## 1. Introduction

Semantic segmentation [1] is a fundamental problem in computer vision, which requires assigning the proper category label to each pixel of a given image. It plays a key role in applications of various domains, including image retrieval,

---

<sup>☆</sup>This research was funded by.

<sup>\*</sup>Corresponding author

*Email addresses:* jizong.peng.1@etsmtl.net (Jizong Peng), guillermo@ele.puc-rio.br (Guillermo Estrada), marco.pedersoli@etsmtl.ca (Marco Pedersoli), christian.desrosiers@etsmtl.ca (Christian Desrosiers)

autonomous driving, video surveillance, remote sensing, robotics and biomedical imaging. This task is particularly important for medical image analysis, where it serves as a necessary pre-processing step for the assessment and treatment planning of various medical conditions [2].

In recent years, supervised approaches, in particular those based on deep learning, have shown tremendous potential for automated image segmentation. In such approaches, parametric models like fully-convolutional neural networks (F-CNNs) [3] are trained with a large set of annotated images by minimizing some loss function like cross-entropy or Dice loss [4]. In many cases, however, obtaining sufficient data for training can be challenging and manually annotating natural images can take up to 2 hours per image [5]. This problem is even more significant in medical imaging applications, where images are typically 3D volumes (e.g., MRI or CT scans), the regions to delineate have low contrast, and annotations must be made by highly-trained experts. For challenging problems like infant brain segmentation, obtaining reliable annotations for a single subject may take a radiologist up to a week<sup>1</sup>.

To alleviate the need for fully-annotated data, numerous works have focused on developing weakly-supervised methods for segmentation. In such methods, easier to obtain annotations like image-level tags [6, 7, 8, 9], bounding boxes [10, 11] or scribbles [12] are used for training segmentation models, instead of whole-image pixel labels. Multiple instance learning (MIL) [13] is a popular technique for dealing with image tags, where images are considered as bags of pixels / superpixels (i.e., instances) and positive examples for a given object of interest (i.e., tag) are images for which at least one pixel / superpixel corresponds to that object. MIL methods for segmentation typically rely on objectness [14, 15, 16, 17, 18, 19], class-specific saliency and activation maps [20, 21, 22, 23], or image-level constraints [8, 9] to obtain a prior on the presence or location of objects in the image.

In various scenarios, weakly-supervised learning methods for segmentation

---

<sup>1</sup>See <http://iseg2017.web.unc.edu/reference/>

may not be suitable. For instance, adding bounding boxes or point annotations can still be time-costly for 3D scans, which may contain over 100 separate images (i.e., 2D slices). Likewise, image-level tags are not very useful in segmentation tasks where one must separate a single region of interest (i.e., foreground) from the background. In contrast, semi-supervised learning methods [24, 25, 26, 27, 28] seek to improve the training of segmentation models by leveraging unlabeled images, in addition to labeled ones. Unlike weakly-supervised approaches, these methods rely on intrinsic properties of the data distribution (or *priors*) which are not specific to individual images. Semi-supervised methods for segmentation include techniques based on self-training [24], model-based [29] or data-based [30, 27] distillation, attention learning [26], adversarial learning [31, 32, 33, 34], and manifold embedding [25].

Co-training is one of the most popular general-purpose techniques for semi-supervised learning. Proposed by Blum and Mitchell in their seminal paper [35], this technique uses the prediction of two complementary classifiers on unlabeled data to simultaneously bootstrap their performance in an iterative manner [36]. While co-training has been used with great success in natural language processing [37, 36, 38], its application to visual tasks has so far been limited [39]. One of the main reasons for this is that standard co-training algorithms require the two complementary models to learn from independent features. While such independent features may be available in specific scenarios (e.g., multiplanar images [27]), there is no effective way to construct these sets from individual images.

Recently, Qiao *et al.* proposed a deep co-training method for semi-supervised image recognition [40]. The main innovation of this work is to use adversarial examples, built from both labeled and unlabeled images, for imposing diversity among the different classifiers. Specifically, during training, a classifier is encouraged to output predictions similar to those of the other classifier for adversarial examples, hence classifiers will tend to disagree for those examples. The two classifiers would thus not collapse to each other. Until now, deep co-training has been applied only to classification. In contrast, semantic segmentation is a

more complex problem, with a larger and structured output space. In this work we extend and adapt the co-training approach for this task. The contributions of our work are as follows:

- We present a deep adversarial co-training method for semantic segmentation, extending the work of Qiao *et al.* to this more challenging problem. To our knowledge, this is the first co-training method proposed for semantic segmentation.
- We conduct a comprehensive set of experiments which demonstrate the potential of co-training for segmenting different types of images. Our experiments also analyze the impact of various elements of the method, including the number of classifiers, the trade-off between model agreement and diversity, and the generation of adversarial examples. We believe these experiments can be of benefit to future investigations on co-training methods for segmentation.

The rest of this paper is as follows. In the next section, we give a brief summary of related literature, focusing on recently proposed methods for semi-supervised segmentation. In Section 3, we present our deep adversarial co-training approach for segmentation. We then evaluate our method on the tasks of segmenting cardiac and spine structures. Finally, we conclude with a summary of our contribution and results.

## 2. Related work

Semi-supervised learning has a long history in machine learning. The first methods were proposed around 50 years ago for estimating mixture models [41, 42]. Since then, many different approaches have been proposed. Here, we will focus mostly on the most recent and promising methods for visual recognition and, more specifically, semantic segmentation. For a complete review of semi-supervised methods, see [43].

A quite simple, yet powerful approach for semi-supervised learning is to select the most likely label of the current model as ground truth for unsupervised data. This is often referred as pseudo-label [44] or entropy regularization [45]. More sophisticated approaches make use of unlabeled samples, leveraging the unsupervised representation of an autoencoder [46] or a variational autoencoder [47]. Another line of research for semi-supervised learning is based on the idea that the pseudo-labeling can be improved and made more robust if multiple models are used for generating the pseudo-labels [48, 49]. Regularizing the learning with adversarial examples is also a promising technique. It consists in generating samples that are adversarial to the model [50], i.e. samples that the model cannot classify correctly, and adding them to the training data to improve robustness. Recently, the generation of adversarial samples has been applied to unlabeled samples, therefore extending their use to semi-supervised learning with very promising results [51]. This technique has also been used for co-training multiple classification models [40]. Our proposed method is based on the last approach, but adapted to the more challenging task of semi-supervised image segmentation. For an updated evaluation of state-of-the art semi-supervised methods for image classification, see [52].

Semi-supervised learning has also been used for image segmentation [24, 25, 26, 27]. As for classification, the main idea of semi-supervised segmentation methods is to propagate the labels of training samples to unlabeled images. However, in the case of segmentation, the output is structured and therefore methods based on local vicinity of the sample representation would not work. A common approach is to use an iterative two steps procedure in which: i) the unlabeled images are annotated considering the output of the segmentation network as ground truth; ii) the network parameters are updated based on the segmented (annotated) images [24]. A common problem of such approach is that initial small errors might be propagated and amplified to unlabeled images, producing catastrophic results. Various approaches are used to avoid this problem. For instance model-based [29] and data-based [30, 27] distillation can reduce the error propagation by aggregating the prediction of multiple teacher

models to train a student model [26]. Another approach proposed by Baur *et al.* [25] embeds the network representation in a manifold, such that images having similar characteristics are near to each other.

Methods based on generative adversarial networks (GANs) [53] have recently shown promising results for semi-supervised segmentation [31, 32, 33, 34]. The first approach using GANs for semantic segmentation was proposed by Luc *et al.* [34] and extended to the semi-supervised case in [33]. In this work, a discriminator network should distinguish between the segmentation of labeled and unlabeled images. This forces the segmentation model to perform as well on unlabeled images, in order to fool the discriminator. An improved strategy is proposed by Hung *et al.* [32], where the discriminator is used to predict areas of high confidence on unlabeled images. These areas are then used to update the segmentation network. It is important to distinguish GAN models from the use of adversarial examples [50]. While GAN models are based on the simultaneous learning of two adversarial networks (the discriminator and the generator), adversarial training proposes the generation of samples with subtle modifications that can fool a learned model. Although GANs have already been employed for improving semi-supervised approaches, adversarial samples have not been applied yet to segmentation. In this paper, we show how to leverage adversarial samples in semi-supervised segmentation by exploiting a co-training procedure [40].

### 3. Methodology

#### 3.1. Co-training basics

Co-training is based on the assumption that training examples can be described by two complementary sets of features called views. In the ideal case, these views should be conditionally independent given the corresponding class labels. In addition, models trained individually on each view should be sufficiently accurate (i.e., it should be possible to learn independently from each view). Unlike standard ensemble learning techniques like bagging [54], where

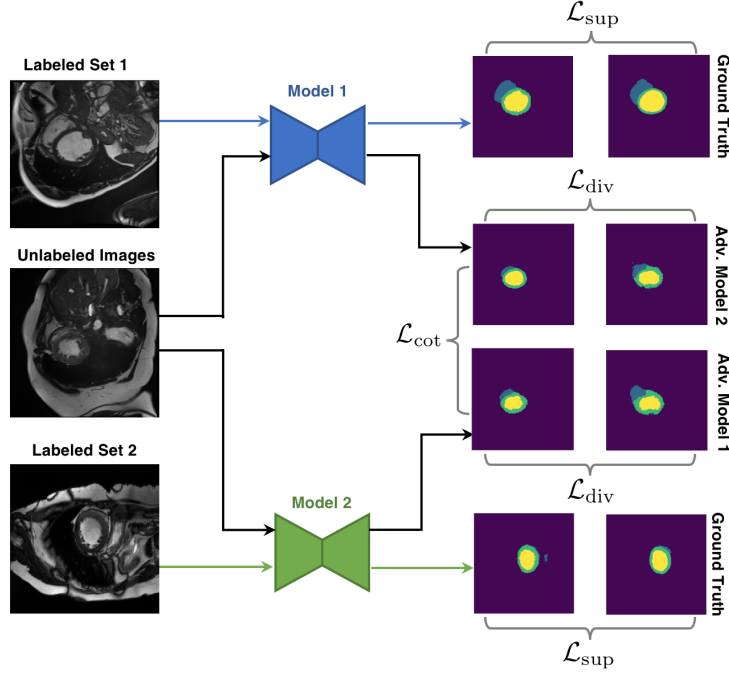


Figure 1: Overview of the deep co-training approach proposed for image segmentation (dual-view setting). Two deep CNNs are trained simultaneously with different sets of labeled images and a common set of unlabeled images. The loss function is composed of three terms:  $\mathcal{L}_{\text{sup}}$ ,  $\mathcal{L}_{\text{cot}}$  and  $\mathcal{L}_{\text{div}}$ . Term  $\mathcal{L}_{\text{sup}}$  ensures that network predictions for labeled examples are consistent with ground truth segmentation masks;  $\mathcal{L}_{\text{cot}}$  forces networks to agree with each other for unlabeled examples;  $\mathcal{L}_{\text{div}}$  imposes a network to agree with the predictions of the other network’s adversarial examples.

models are trained separately and a prediction is obtained by combining the output of trained models (e.g., majority vote), co-training seeks to train different models in a collaborative way so that they can learn from one another. In the original method proposed by Blum and Mitchell [35], a separate classifier is learned for each view using labeled data. The most confident predictions of each classifier on unlabeled examples are then used iteratively as additional labeled examples in the training set of the other classifier. Multi-view co-training (or multi-view learning) [55] extends this idea to multiple complementary views. The general principle of this type of method is to simultaneously train clas-

sifiers for each view, using the labeled data, such that their predictions agree for unlabeled examples. Enforcing this agreement between classifiers reduces the search space and, thus, helps finding a model which will generalize well to unseen data.

### 3.2. Problem formulation

As a dense prediction problem with complex output space, semantic segmentation is extremely challenging in a semi-supervised setting. In real-life applications, particularly those related to medical imaging, such a setting is however common since manual annotation is often an expensive and time-consuming process. Consequently, only a small fraction of images in the dataset can have full pixel-wise labels. The proposed method aims to exploit both labeled and unlabeled images by using the general, yet powerful principle of multi-view co-training.

We formalize the problem of image segmentation as follows. Given a set of labeled data  $\mathcal{S} = \{(x_1, y_1), \dots, (x_m, y_m)\}$ , each example comprised of an image  $x_i : \Omega \rightarrow \mathcal{F}$  and corresponding ground truth segmentation mask  $y : \Omega \rightarrow \mathcal{C}$ , where  $\Omega$  is the set of image pixels (or voxels in the 3D case),  $\mathcal{F}$  the set of pixel features (e.g.,  $\mathcal{F} = \mathbb{R}$  for grey-scale images), and  $\mathcal{C}$  the set of possible labels. In a semi-supervised setting, we also have a set of  $n$  unlabeled images  $\mathcal{U} = \{x_1, \dots, x_n\}$ , with  $n \gg m$ , without ground truth labels. The goal is to learn from  $\mathcal{D} = \mathcal{S} \cup \mathcal{U}$  a segmentation model  $f$ , parametrized by  $\theta$ , which maps each pixel of an input image to its correct label.

### 3.3. Proposed approach

As in standard multi-view learning approaches, we train multiple models in a collaborative manner and, once trained, combine their outputs to predict the labels of new images. Motivated by the outstanding performance of deep convolutional network networks (CNNs) for various segmentation tasks [56, 57, 58], we employ this type of model in the proposed approach. Specifically, we train an ensemble of  $k$  segmentation networks  $f^i(\cdot; \theta^i)$ ,  $i = 1, \dots, k$ . We assume

the network output as softmax selecting a class for each pixel of the image and denote as  $f_{jc}^i$  the probability of label  $c$  for pixel  $j$ , predicted by ensemble model  $i$ . Without loss of generality, in what follows, we will consider a dual view setting (i.e.,  $k = 2$ ) and describe how this setting can be naturally extended to multiple views.

Following the recent work of Qiao *et al.* on deep co-training image classification [40], we employ a loss function composed of a weighted sum of three separate terms to train the ensemble’s segmentation models (see Fig. 1):

$$\mathcal{L}(\theta; \mathcal{D}) = \mathcal{L}_{\text{sup}}(\theta; \mathcal{S}) + \lambda_{\text{cot}} \mathcal{L}_{\text{cot}}(\theta; \mathcal{U}) + \lambda_{\text{div}} \mathcal{L}_{\text{div}}(\theta; \mathcal{D}). \quad (1)$$

The three loss terms are explained in following subsections.

### 3.3.1. Supervised loss

The first term,  $\mathcal{L}_{\text{sup}}$ , is the supervised loss obtained from labeled examples. It aggregates the loss computed separately for each model:

$$\mathcal{L}_{\text{sup}}(\theta; \mathcal{S}) = \mathcal{L}_{\text{sup}}^1(\theta^1; \mathcal{S}^1) + \mathcal{L}_{\text{sup}}^2(\theta^2; \mathcal{S}^2), \quad (2)$$

Here, labeled data subsets  $\mathcal{S}^i \subset \mathcal{S}$ ,  $i \in \{1, 2\}$  can differ across models to ensure their diversity. While any segmentation loss can be considered, in this work, we employed the well-known pixel-wise cross-entropy loss, defined as

$$\mathcal{L}_{\text{sup}}^i(\theta^i; \mathcal{S}^i) = \mathbb{E}_{(x,y) \in \mathcal{S}^i} \left[ \sum_{j \in \Omega} \sum_{c \in \mathcal{C}} y_{jc} \log f_{jc}^i(x; \theta^i) \right], \quad (3)$$

where  $y_{jc} = 1$  if the label of pixel  $j$  is  $c$ , else  $y_{jc} = 0$  (i.e., one-hot label encoding). Supervised loss  $\mathcal{L}_{\text{sup}}$  encourages models to output consistent predictions with respect to their ground truth labels.

### 3.3.2. Ensemble agreement loss

In addition to exploiting labeled information, unlabeled image dataset  $\mathcal{U}$  is also used to guide the learning process. Based on the consensus principle [55], we want the segmentation networks to output similar predictions for the same unlabeled images. We argue that enforcing this agreement helps improve the

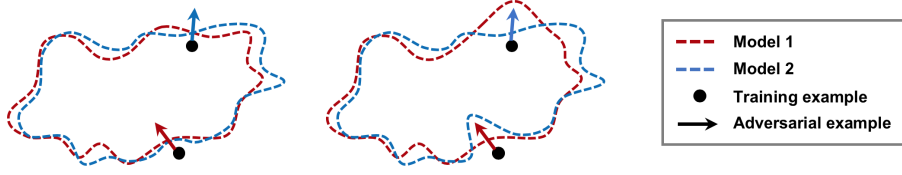


Figure 2: Illustration of the ensemble diversity strategy based on adversarial training. Adversarial examples are generated from training images (black dots), for both models (red and blue arrows). Each model is then forced to agree with the prediction of the other model for its own adversarial examples (right-side image).

generalization of individual models by restricting their parameter search space to cross-view consistent solutions. Toward this goal, we minimize the distance between the class distributions predicted by different models. To make our approach compatible with more than two views, we define the agreement loss  $\mathcal{L}_{\text{cot}}$  as the Jensen-Shannon divergence (JSD), which is the average Kullack-Liebler divergence  $D_{\text{KL}}$  between the prediction of each model  $f^i$  and their mean prediction  $\bar{f}$ :

$$\begin{aligned} \mathcal{L}_{\text{cot}}(\theta; \mathcal{U}) &= \mathbb{E}_{x \in \mathcal{U}} \left[ D_{\text{KL}}\left(f^1(x; \theta^1) \parallel \bar{f}(x; \theta)\right) + D_{\text{KL}}\left(f^2(x; \theta^2) \parallel \bar{f}(x; \theta)\right) \right] \\ &= \mathbb{E}_{x \in \mathcal{U}} \left[ \mathcal{H}\left(\frac{1}{2}(f^1(x; \theta^1) + f^2(x; \theta^2))\right) - \frac{1}{2}\left(\mathcal{H}(f^1(x; \theta^1)) + \mathcal{H}(f^2(x; \theta^2))\right) \right]. \end{aligned} \quad (4)$$

In this equation,  $\mathcal{H}(\cdot)$  corresponds to the Shannon entropy. Unlike KL divergence, the JSD between different distributions is symmetric, and thus loss  $\mathcal{L}_{\text{cot}}$  considers the prediction of all models equally important when minimizing their disagreement.

### 3.3.3. Diversity loss

A key principle of ensemble learning is having diversity between models in the ensemble. If all models learn the same class distribution, then combining their output will not be superior to individual model predictions. In co-training, diversity is essential so that models can learn from one another during training. The standard approach for obtaining diversity is to have independent sets

of features (i.e., views), or generating them by splitting available features into complementary subsets. In deep CNN classification, however, the internal representation of images is learned by the network during training, therefore such standard approach cannot be applied.

Since models in the ensemble must agree for unlabeled images, and their prediction on labeled images is constrained by ground-truth segmentation masks, training images cannot be used directly to impose diversity. Instead, we use the approach proposed by Qiao *et al.* image for classification [40], and augment the dataset with adversarial examples generated from both labeled and unlabeled data. Adversarial examples for a model are used to teach other models in the ensemble. In the case of dual-view co-training, we define our diversity loss as

$$\mathcal{L}_{\text{div}}(\theta; \mathcal{D}) = \mathbb{E}_{x \in \mathcal{D}} \left[ \mathcal{H}\left(f^1(x; \theta^1), f^2(g^1(x); \theta^2)\right) + \mathcal{H}\left(f^2(x; \theta^2), f^1(g^2(x); \theta^1)\right) \right], \quad (5)$$

where  $\mathcal{H}(\cdot, \cdot)$  refers to cross-entropy and  $g^i(x)$  is an adversarial example targeted on model  $f^i(\cdot; \theta^i)$ , given input image  $x$ . As illustrated in Fig. 2, this loss function encourages a model to be robust to the adversarial examples generated for the other one, thereby avoiding the collapse of their decision boundary on each other (i.e., the adversarial loss reaches its maximum when the two networks are identical).

The diversity imposed by the loss can also be motivated as follows. If example  $g^1(x)$  is adversarial for model 1, then we have that  $f^1(x; \theta^1) \neq f^1(g^1(x); \theta^1)$ . Moreover, minimizing the first term of Eq. (5) will impose that  $f^1(x; \theta^1) = f^2(g^1(x); \theta^2)$ . Last, combining both relations yields  $f^1(g^1(x); \theta^1) \neq f^2(g^1(x); \theta^2)$ . Applying the same idea for model 2, we conclude that models will disagree on adversarial examples of each model. One should note, however, that the above relations are not guaranteed to hold in practice (e.g., predictions can be very similar but not equal). In our experiments, we show that differences mostly occur on the boundary between different regions, which is where most segmentation mistakes are made.

Adversarial examples are generated by adding small perturbations to in-

put images, so as to change the network’s prediction as much as possible. In this work, we generate these examples using distinct schemes depending on the source of the image  $x$ . If  $x$  is drawn from the unlabeled dataset  $\mathcal{U}$ , we apply the Virtual Adversarial Training (VAT) [59] method because no ground truth is available. VAT optimizes local distribution smoothness (LDS) which measures the robustness of the model against virtual adversarial direction. We following the same strategy as in VAT to generate an adversarial example  $x_{\text{adv}} = x + r_{\text{adv}}$  from a training images  $x$ :

$$r_{\text{adv}} = \arg \max_{r; \|r\|_2 \leq \epsilon} D_{\text{KL}}(f(x; \theta) \parallel f(x + r; \theta)). \quad (6)$$

On the other hand, when  $x$  is drawn from the labeled set  $\mathcal{S}$ , we instead apply the Fast Gradient Sign Method (FGSM) since it can produce noise targeted to the ground truth, thus providing more valuable information. In this case, adversarial examples  $x_{\text{adv}}$  are generated by FGSM as

$$x_{\text{adv}} = x + \epsilon \cdot \text{sign}\left(\nabla_x \mathcal{H}(f(x; \theta), y)\right), \quad (7)$$

where  $\mathcal{H}$  is the cross-entropy loss used as in full supervision, and  $y$  is the true label of  $x$ . This approach also constrains the magnitude of adversarial perturbation using a predefined  $\epsilon$  parameter.

## 4. Experiments and results

### 4.1. Evaluation datasets and metrics

Our experiments are conducted on two semantic segmentation datasets: Automated Cardiac Diagnosis Challenge (ACDC) [60] and Spinal Cord Gray Matter Challenge (SCGM) [61].

- **ACDC dataset:** The publicly available ACDC dataset consists of 200 short-axis cine-MRI scans from 100 patients, evenly distributed in 5 subgroups: normal, myocardial infarction, dilated cardiomyopathy, hypertrophic cardiomyopathy, and abnormal right ventricles. Scans correspond to end-diastolic (ED) and end-systolic (ES) phases, and were acquired on

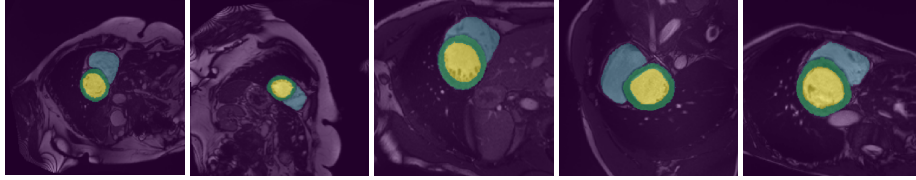


Figure 3: Examples of images and ground truth segmentation masks in the ACDC dataset. Images are segmented in four separate classes: endocardium of the left ventricle (LV, yellow), myocardium of the left ventricle (Myo, green), endocardium of the right ventricle (RV, blue), background (purple).

1.5T and 3T systems with resolutions ranging from  $0.70 \times 0.70$  mm to  $1.92 \times 1.92$  mm in-plane and 5 mm to 10 mm through-plane. Segmentation masks delineate 4 regions of interest: left ventricle endocardium (LV), left ventricle myocardium (Myo), right ventricle endocardium (RV), and background (see Fig. 3). For our experiments, we used a split with 175 scans for training and 25 for testing. Short-axis slices within 3D-MRI scans were considered as 2D images, which were re-sized to  $256 \times 256$ .

- **SCGM dataset:** The SPGM dataset is a publicly-available collection of multi-center, multi-vendor MRI. It comprises a total of 80 healthy subjects (age range of 28.3 to 44.3 years) obtained by four different centers, with 20 subjects from each center. Scans were acquired using different MRI systems and distinct acquisition parameters, leading to high-variability of image characteristics: resolution range of  $0.25 \times 0.25 \times 2.5$  mm to  $0.5 \times 0.5 \times 5.0$  mm, number of axial slices range of 3 to 28. The training set contains 40 labeled scans, each annotated slice-wise by 4 independent experts and the ground truth mask obtained by majority voting. Ground truth labels for the remaining 40 test images are not available. For additional details on the dataset, see [61].

In [28], this dataset is used to train and test a semi-supervised segmentation method based on the mean teacher algorithm. Experiments of this work, which focused on domain adaptation, used images from centers 1

and 2 as the training set, images from center 3 as the validation set, and images from center 4 as the test set. In our work, we seek to evaluate methods in a more traditional semi-supervised setting, where very few labeled images are seen in training. Hence, we consider a different training set where labeled images only come from center 1 (total of 30 images), and unlabeled images from all centers are used (total of 465 images). The test set contains labeled images from centers 3 and 4 (total of 264 images). Following [28], slices in each scan are first resampled to a uniform resolution of  $0.25 \times 0.25$  mm, and then center-cropped to a size of  $200 \times 200$  pixels.

We use the Dice similarity coefficient (DSC) to evaluate the performance of a segmentation model, which is defined as

$$\text{DSC}(A, B) = \frac{2|A \cap B|}{|A| + |B|}. \quad (8)$$

This well-known metric measures the overlap between the predicted and ground truth segmentation.

#### 4.2. Experimental details

As segmentation network, we employed the well-known U-Net [62] architecture, with 15 layers, Dropout and ReLU activations. This architecture is one of the most popular models for segmentation, especially for tasks related to bio-medical imaging. The same data augmentation strategy was considered for both datasets, which applies random rotation, flip, and random crop of 85-95% surface on the original image.

Networks were trained using stochastic gradient descent (SGD) with the Adam optimizer. Learning parameters were set separately for each dataset. For ACDC, we used a maximum number of epochs of 120, initial learning rate of 0.001 and weight decay of 0.0001. The learning rate was decreased by a factor of 10 every 30 epochs. Batch size was set to 4 for both labeled and unlabeled data. FSGM with  $\epsilon = 0.03$  was used to create adversarial examples (corresponding to a maximum perturbation of 3% for each pixel). For SCGM, the maximum

number of epochs was set to 300, and learning rate decreased by a factor of 10 each 100 epochs. All other parameters remained the same for this dataset.

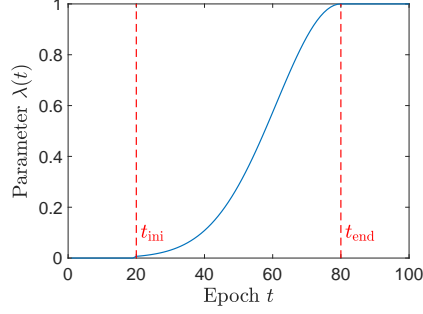


Figure 4: Example of ramp-up function  $\lambda(t)$  for  $\lambda_{\max} = 1$ ,  $t_{\text{ini}} = 20$  and  $t_{\text{end}} = 80$ .

For all running experiments, we used a dynamic strategy to set the value of both  $\lambda_{\text{cot}}$  and  $\lambda_{\text{div}}$  parameters in Eq. (1). This strategy follows a Gaussian ramp-up curve defined by parameters  $\lambda_{\max}$ ,  $t_{\text{ini}}$  and  $t_{\text{end}}$ :

$$\lambda(t) = \begin{cases} 0 & , \text{ if } t < t_{\text{ini}} \\ \lambda_{\max} \cdot \exp\left(-5 \cdot \left(1 - \frac{t - t_{\text{ini}}}{t_{\text{end}} - t_{\text{ini}}}\right)^2\right) & , \text{ if } t_{\text{ini}} \leq t < t_{\text{end}} \\ \lambda_{\max} & , \text{ if } t \geq t_{\text{end}} \end{cases} \quad (9)$$

To avoid hampering training in its early stage, we only apply the ramp-up function after  $t_{\text{ini}}$  epochs. For  $\lambda_{\text{cot}}$  we set  $t_{\text{ini}}$  to 1, while for  $\lambda_{\text{div}}$  we set it to 20, since adversarial noise is meaningless if networks are in the beginning of the training. In experiments, we fix  $t_{\text{end}} = 50$  for both  $\lambda_{\text{cot}}$  and  $\lambda_{\text{div}}$ . The maximum value of  $\lambda_{\text{cot}}$  and  $\lambda_{\text{div}}$  is controlled by ramp-up parameter  $\lambda_{\max}$ , which we set to 0.5 for  $\lambda_{\text{cot}}$  and 0.05 for  $\lambda_{\text{div}}$ .

We report the average performance of individual models, as well as the performance of soft voting on all available models. Soft-voting is commonly used in homogeneous ensemble techniques like bootstrap aggregating (bagging). It consists in averaging the pixel-wise class probabilities across models, and using this average as ensemble prediction. In our experiments, we observed that soft-voting usually outperforms hard-voting, where the ensemble’s label is the one predicted by the majority of models (with random tie-breaking), and thus only

considered the former.

Our deep co-training method is also compared against a recent approach based on the mean teacher algorithm [28]. To our knowledge, this is the only other approach using multiple deep CNNs for semi-supervised segmentation. For this baseline, we follow the same optimization, learning rate decay, weight scheduler, and data augmentation setting as for our method. As in [28], data augmentation is applied to input images of a student model. Non-augmented images are fed to a teacher model, whose parameters  $\theta'$  are computed by running an exponential moving average (EMA) on the student’s parameters  $\theta$ :

$$\theta'_t = \alpha\theta'_{t-1} + (1 - \alpha)\theta_t. \quad (10)$$

In our experiments, we set  $\alpha$  to 0.99. Finally, the student’s output for augmented images is forced to be consistent with the teacher’s prediction, augmented using the same strategy, via an  $L_2$  loss.

### 4.3. Experimental results

#### 4.3.1. ACDC dataset

We first evaluate our deep co-training method on the ACDC dataset using a dual view setting, i.e., training two segmentation models using the proposed loss. Performance is reported as the average of DSC scores over the two models, and the DSC obtained by combining obtained model predictions with soft-voting. To simulate different levels of supervision, we vary the ratio of labeled images in the training set,  $l_a$ ,  $0 \leq l_a \leq 1$ . Images and ground-truth segmentation masks from the first  $l_a \times 100$  training patients are used as labeled data, while the images of remaining patients serve as unlabeled data.

As baseline, we trained the two models independently, without considering the ensemble agreement (i.e.,  $\mathcal{L}_{\text{cot}}$ ) or adversarial diversity (i.e.,  $\mathcal{L}_{\text{div}}$ ) loss terms. In the presentation of results, this baseline is referred to as Partial. Note that the soft-voting score of this baseline corresponds to the well-known bagging technique in ensemble learning. As fully-supervised baseline, we also report the DSC obtained by training a single model with all available training examples.

Table 1: DSC performance of tested methods for validation images of the ACDC dataset. Except for full-supervision, all methods were trained with 20% of labeled data. Partial ( $\mathcal{L}_{\text{sup}}$  only), JSD ( $\mathcal{L}_{\text{sup}} + \mathcal{L}_{\text{cot}}$ ) and DCT-Seg ( $\mathcal{L}_{\text{sup}} + \mathcal{L}_{\text{cot}} + \mathcal{L}_{\text{div}}$ ) were trained in a dual-view setting, each model using the same set of labeled images. For these methods, we report the average ensemble performance and the DSC obtained by combining ensemble predictions with soft-voting. Note: reported values are the average of DSC measures for two separate runs, each one with a different random seed.

Method		Myo	RV	LV	Mean
Partial	avg.	63.311	78.301	86.194	75.935
	voting	62.893	79.669	86.960	76.507
JSD	avg.	66.380	79.248	89.605	78.411
	voting	66.144	80.420	<b>90.604</b>	79.056
DCT-Seg	avg.	74.784	80.817	88.927	81.509
	voting	<b>75.770</b>	<b>81.648</b>	89.606	<b>82.342</b>
Mean Teacher [28]		73.735	75.066	83.755	77.519
Full		81.784	85.757	92.185	86.575

This baseline is denoted as Full in results. Moreover, to measure the relative contribution of the adversarial loss terms on performance, we also give the average and soft-voting score of the ensemble trained without this term, and denote this approach as JSD in the results. The proposed method, which combines all three loss terms, is referred to as DCT-Seg.

Table 1 gives the class-wise mean DSC of tested methods for a labeled data ratio of  $l_a = 0.2$ . To evaluate robustness against parameter initialization, we ran the experiment twice with different random seeds, and computed the average DSC over the two runs. We report both the ensemble average score (avg. in the table) and the DSC obtained by ensemble soft-voting (voting in the table). As expected, ensemble soft-voting leads to a higher DSC than the prediction of individual models in all cases. This confirms the benefit of aggregating predictions from different models. It can also be observed that considering ensemble agree-

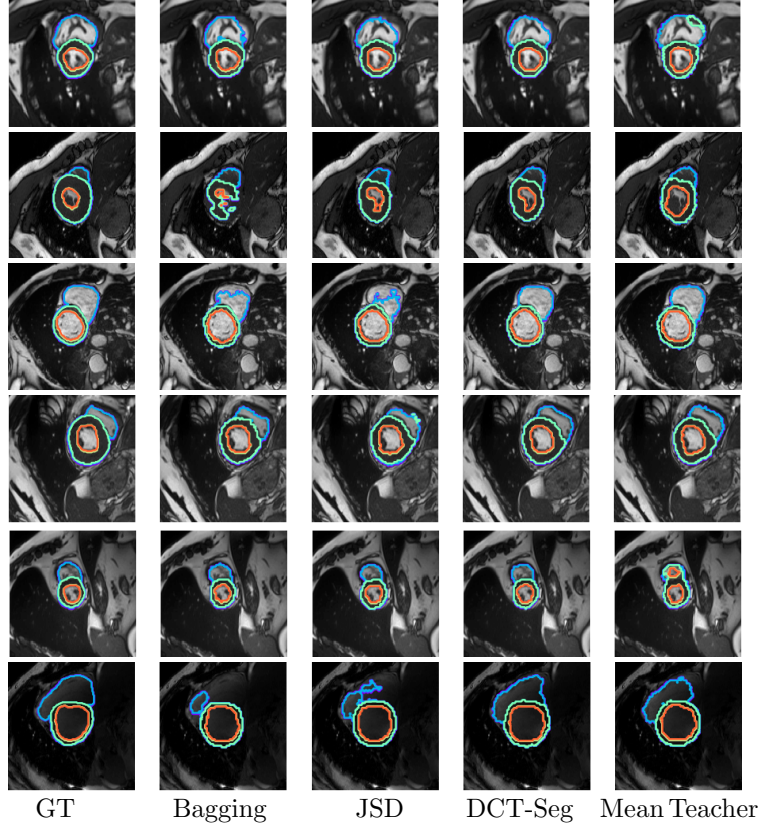


Figure 5: Examples of segmentation results for the ACDC dataset with 20% of labeled training examples. From left to right: ground-truth (GT), ensemble bagging, JSD only, DCT-Seg (JSD + Adv) and Mean Teacher [28].

ment without diversity (JSD) leads to a higher accuracy than the supervised loss alone (Partial). However, combining all three losses in DCT-Seg gives the best performance, with overall mean DSC improvements of 5.835% compared to Partial and 4.823% over Mean Teacher. While only 20% of training images were labeled, DCT-Seg achieved a performance 95% that of full-supervision. Examples of segmentation results for tested methods are shown in Fig. 5. We see that deep co-training gives contours closer to the ground-truth, with very few artifacts on the boundaries between different regions.

Next, we assess whether having more models in the ensemble (i.e., more

Table 2: DSC performance on the ACDC validation set when training different numbers of segmentation models (i.e., views) separately (Partial) or with the proposed deep co-training method (DCT-Seg). In this experiment, 20% of training images are labeled. Note: differences with Table 1 for the dual-view setting are due to the use of different random seeds in this experiment.

Method		2 views	3 views	4 views
Partial	avg.	74.463	72.447	73.236
	voting	75.504	73.900	75.194
DCT-Seg	avg.	79.888	80.094	79.942
	voting	<b>80.565</b>	<b>81.360</b>	<b>81.219</b>

Table 3: DSC performance on the ACDC validation set when training two segmentation models separately (Partial) or with the proposed deep co-training method (DCT-Seg), for three different ratios  $l_a$  of labeled examples.

Method		$l_a = 10\%$	$l_a = 20\%$	$l_a = 50\%$
Partial	avg.	70.709	75.935	83.810
	voting	71.959	76.507	84.398
DCT-Seg	avg.	76.532	81.509	84.165
	voting	<b>77.263</b>	<b>82.342</b>	<b>85.255</b>

than two views) can further boost performance of methods. Toward this goal, we repeat the experiment with 2, 3 and 4 views, once more using a labeled image ratio of  $l_a = 0.2$ . The overall mean DSC of tested methods, computed over the all classes, is reported in Table 2. We see that increasing the number of views does not improve performance for individually-trained models (Partial). On the other hand, for deep co-training, a small increase in DSC is observed when going from 2 to 3 views. However, adding a fourth view does not further improve performance, suggesting that co-training can effectively capture variability with a very limited number of views.

As third experiment, we evaluate how the proportion of labeled data impacts

Table 4: DSC performance of tested methods for validation images of the SCGM dataset. Partial ( $\mathcal{L}_{\text{sup}}$  only), JSD ( $\mathcal{L}_{\text{sup}}+\mathcal{L}_{\text{cot}}$ ) and DCT-Seg ( $\mathcal{L}_{\text{sup}}+\mathcal{L}_{\text{cot}}+\mathcal{L}_{\text{div}}$ ) were trained in a dual-view setting, each model using the same set of labeled images. For these methods, we report the average ensemble performance and the DSC obtained by combining ensemble predictions with soft-voting. Note: reported values are the average of DSC measures for two separate runs, each one with a different random seed.

Method		DSC
Partial	avg.	43.310
	voting	43.225
JSD	avg.	45.589
	voting	44.957
DCT-Seg	avg.	71.087
	voting	<b>72.763</b>
Mean Teacher [28]		50.548

results in a dual-view setting. Table 3 gives the performance of individually-trained models (Partial) and co-training for three labeled data ratio: 10%, 20% and 50%. A clear trend is observed in these results, where mean DSC values increase sharply with the ratio of labeled images in training. In all cases, deep co-training leads to a higher DSC than training models separately, the most significant improvements obtained for the smallest ratio of  $l_a = 10\%$ . Interestingly, DSC improvements near 1% are provided by deep co-training even when half training images are labeled (i.e.,  $l_a = 50\%$ )

#### 4.3.2. SCGM dataset

To further validate the effectiveness of our proposed deep co-training method, we evaluated it on the task of segmenting spinal chord grey matter in images from the SCGM dataset. As mentioned previously, this experiment aims at testing our method in a challenging setting where very few labeled images are used in training (i.e., only 30 images), and test images were generated using different acquisition parameters.

Results of this experiment are summarized in Table 4. Important differences can be observed between the DSC of tested methods. In this case, JSD improves the results of Partial only slightly, while deep co-training increases DSC scores of both these methods by nearly 25%. This suggests that adversarial learning is highly useful when supervised training is limited (i.e., few labeled training examples, different from test examples). In comparison, Mean Teacher provides a DSC improvement of about 5%. The accuracy of deep co-training can be appreciated in Fig. 6, which shows examples of segmentation results for tested methods.

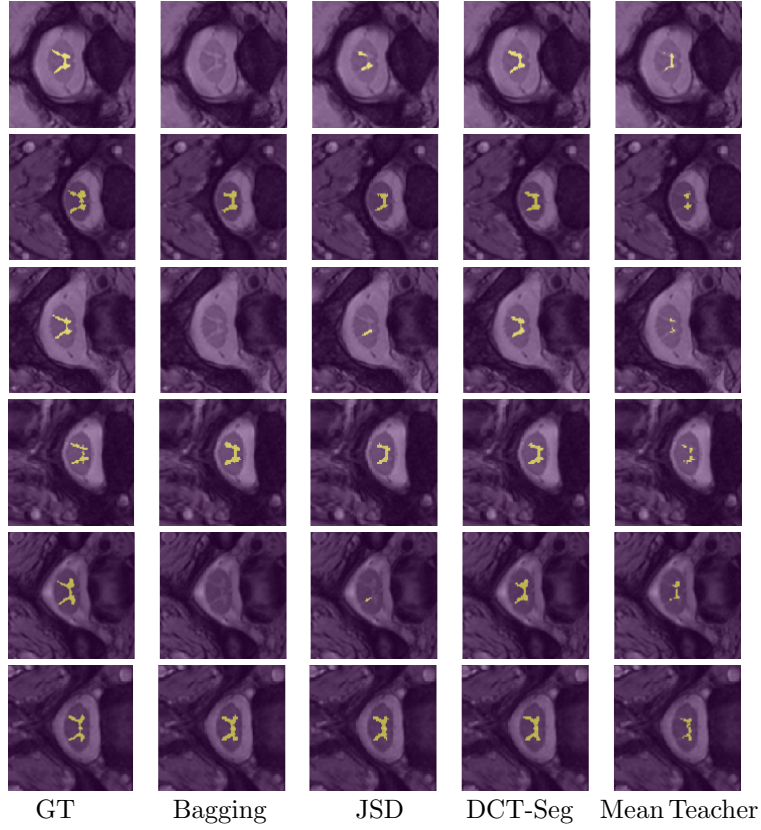


Figure 6: Examples of segmentation results for the SCGM dataset using Center 1 as training data. From left to right: ground-truth (GT), ensemble bagging, JSD only, DCT-Seg (JSD + Adv) and Mean Teacher [28].

#### 4.4. Impact of diversity loss

We investigate the role of the ensemble diversity loss (i.e.,  $\mathcal{L}_{\text{div}}$ ) in our deep co-training method and experimentally show that it also acts as a coarse measure of model agreement, merging the prediction of models while avoiding them to collapse on each other. We perform our investigation on the ACDC dataset using two models. The first one is pre-trained by full supervision as a fixed reference, and the second one trained from scratch using a labeled data ratio of 50%. Note that the trained model is only linked to the fixed reference by  $\mathcal{L}_{\text{div}}$ , and no supervised loss is considered while training this model. Moreover, to measure the impact of adversarial noise  $\epsilon$  in  $\mathcal{L}_{\text{div}}$ , we repeat training with different values for  $\epsilon$ .

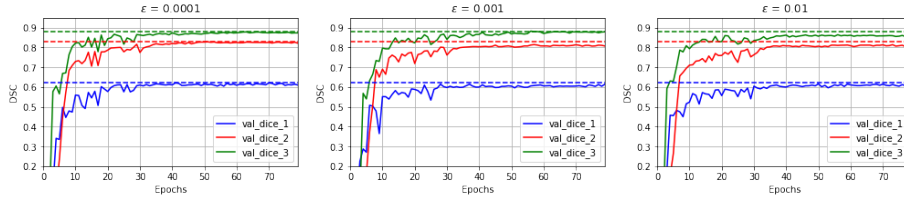


Figure 7: DSC score for models trained from scratch using only  $\mathcal{L}_{\text{div}}$  with different  $\epsilon$ . It is shown that  $\mathcal{L}_{\text{div}}$  plays as a similarity loss especially when  $\epsilon$  is small.

Fig. 7 gives the DSC obtained on the validation set by the reference model (dashed line) and model trained from scratch (solid line), for increasing amounts of adversarial noise  $\epsilon$ . It can be observed that the trained model rapidly converges to the reference, without the need for a supervised signal or specific agreement loss. However, upon convergence, we see that the trained model does not fully reach the accuracy of the reference model, and that the gap between the two models is proportional to the value of  $\epsilon$ . For example, a gap of 1.43%, 1.38% and 0.02% is obtained for the Myo class, when using an  $\epsilon$  of 0.01, 0.001, and 0.0001, respectively. This can be explained by the fact that, when  $\epsilon$  is small, adversarial examples are very similar to original images and  $\mathcal{L}_{\text{div}}$  then acts a symmetric KL loss between the two models.

We then tested the behavior of  $\mathcal{L}_{\text{div}}$  when models are trained simultaneously.

Toward this goal, we initialized the two models using the same fully-supervised checkpoint and linked them only using  $\mathcal{L}_{\text{div}}$ . For a very small  $\epsilon = 1 \times 10^{-3}$ , the DSC of both networks decreases by about 8% percent. When increasing  $\epsilon$ , the DSC for the Myo and RV classes then drops significantly, indicating that these classes are most susceptible to adversarial examples. In order to quantify the diversity of models, we calculated the Cohen Kappa score of their predictions on the validation set (a higher value corresponds to a greater similarity). Since their weights are initialized identically, models have a high Kappa score at the start of training. Then, as training progresses, Kappa scores drop rapidly, suggesting that  $\mathcal{L}_{\text{div}}$  enforces diversity between models, and then stabilize after several epochs. Examples of prediction disagreement, measured by the  $L_1$  norm, are shown in Fig. 8. It can be observed that most differences in predictions occur at the boundary of regions and within regions most difficult to segment (i.e., left ventricle myocardium and right ventricle endocardium).

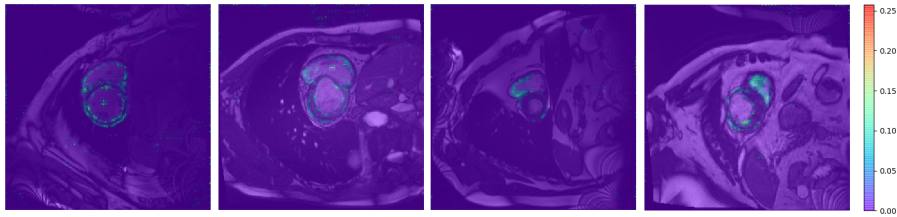


Figure 8: Examples of prediction disagreement between two models linked with the ensemble diversity loss ( $\mathcal{L}_{\text{div}}$ ), measure using  $L_1$  norm.

## 5. Conclusion

We proposed the first application of deep co-training to image segmentation and demonstrated its usefulness on two public benchmark datasets. Our experiments showed that both ensemble agreement and diversity loss terms helped boost performance compared to standard techniques such as bagging, and that combining both in a deep co-training algorithm outperforms recent approaches like Mean Teacher.

In this work, an adversarial learning technique was employed to enforce diversity in the ensemble models. As shown in our results, this technique can also push the predictions of models toward each other, and generates differences mostly in hard-to-segment regions. As future work, it would be interesting to explore a broader range of strategies to create diversity, for example using fake images from generative adversarial networks. Moreover, our experiments revolved around two different medical image segmentation problems. As motivated in the introduction, semi-supervised learning is most important for this type of problems, where annotating images is complex and expensive. Nevertheless, evaluating the proposed method on additional types of images and segmentation tasks would be beneficial.

## References

## References

- [1] H. Noh, S. Hong, B. Han, Learning deconvolution network for semantic segmentation, in: Proceedings of the IEEE international conference on computer vision, 2015, pp. 1520–1528.
- [2] G. J. S. Litjens, T. Kooi, B. E. Bejnordi, A. A. A. Setio, F. Ciompi, M. Ghafoorian, J. A. W. M. van der Laak, B. van Ginneken, C. I. Sánchez, A survey on deep learning in medical image analysis, *Medical Image Analysis* 42 (2017) 60–88. doi:10.1016/j.media.2017.07.005.
- [3] J. Long, E. Shelhamer, T. Darrell, Fully convolutional networks for semantic segmentation, in: Proceedings of the IEEE conference on computer vision and pattern recognition, 2015, pp. 3431–3440.
- [4] F. Milletari, N. Navab, S.-A. Ahmadi, V-net: Fully convolutional neural networks for volumetric medical image segmentation, in: 3D Vision (3DV), 2016 Fourth International Conference on, IEEE, 2016, pp. 565–571.

- [5] A. Kolesnikov, C. H. Lampert, Seed, expand and constrain: Three principles for weakly-supervised image segmentation, in: European Conference on Computer Vision, Springer, 2016, pp. 695–711.
- [6] P. O. Pinheiro, R. Collobert, Weakly supervised semantic segmentation with convolutional networks, in: CVPR, Vol. 2, Citeseer, 2015, p. 6.
- [7] G. Papandreou, L.-C. Chen, K. Murphy, A. L. Yuille, Weakly-and semi-supervised learning of a deep CNN for semantic image segmentation, arXiv preprint arXiv:1502.02734.
- [8] H. Kervadec, J. Dolz, M. Tang, E. Granger, Y. Boykov, I. B. Ayed, Constrained-cnn losses for weakly supervised segmentation, Medical image analysis.
- [9] D. Pathak, P. Krahenbuhl, T. Darrell, Constrained convolutional neural networks for weakly supervised segmentation, in: Proceedings of the IEEE international conference on computer vision, 2015, pp. 1796–1804.
- [10] J. Dai, K. He, J. Sun, Boxsup: Exploiting bounding boxes to supervise convolutional networks for semantic segmentation, in: Proceedings of the IEEE International Conference on Computer Vision, 2015, pp. 1635–1643.
- [11] M. Rajchl, M. C. Lee, O. Oktay, K. Kamnitsas, J. Passerat-Palmbach, W. Bai, M. Damodaram, M. A. Rutherford, J. V. Hajnal, B. Kainz, et al., Deepcut: Object segmentation from bounding box annotations using convolutional neural networks, IEEE transactions on medical imaging 36 (2) (2017) 674–683.
- [12] D. Lin, J. Dai, J. Jia, K. He, J. Sun, Scribblesup: Scribble-supervised convolutional networks for semantic segmentation, in: Proceedings of the IEEE Conference on Computer Vision and Pattern Recognition, 2016, pp. 3159–3167.
- [13] A. Vezhnevets, J. M. Buhmann, Towards weakly supervised semantic segmentation by means of multiple instance and multitask learning, in: Pro-

- ceedings of the IEEE Conference on Computer Vision and Pattern Recognition, IEEE, 2010, pp. 3249–3256.
- [14] A. Bearman, O. Russakovsky, V. Ferrari, L. Fei-Fei, Whats the point: Semantic segmentation with point supervision, in: European Conference on Computer Vision, Springer, 2016, pp. 549–565.
  - [15] Y. Wei, X. Liang, Y. Chen, Z. Jie, Y. Xiao, Y. Zhao, S. Yan, Learning to segment with image-level annotations, *Pattern Recognition* 59 (2016) 234–244.
  - [16] P. O. Pinheiro, R. Collobert, From image-level to pixel-level labeling with convolutional networks, in: Proceedings of the IEEE Conference on Computer Vision and Pattern Recognition, 2015, pp. 1713–1721.
  - [17] X. Qi, Z. Liu, J. Shi, H. Zhao, J. Jia, Augmented feedback in semantic segmentation under image level supervision, in: European Conference on Computer Vision, Springer, 2016, pp. 90–105.
  - [18] F. Saleh, M. S. Aliakbarian, M. Salzmann, L. Petersson, S. Gould, J. M. Alvarez, Built-in foreground/background prior for weakly-supervised semantic segmentation, in: European Conference on Computer Vision, Springer, 2016, pp. 413–432.
  - [19] W. Shimoda, K. Yanai, Distinct class-specific saliency maps for weakly supervised semantic segmentation, in: European Conference on Computer Vision, Springer, 2016, pp. 218–234.
  - [20] Q. Hou, M.-M. Cheng, X. Hu, A. Borji, Z. Tu, P. Torr, Deeply supervised salient object detection with short connections, in: 2017 IEEE Conference on Computer Vision and Pattern Recognition (CVPR), IEEE, 2017, pp. 5300–5309.
  - [21] N. Liu, J. Han, Dhsnet: Deep hierarchical saliency network for salient object detection, in: Proceedings of the IEEE Conference on Computer Vision and Pattern Recognition, 2016, pp. 678–686.

- [22] R. R. Selvaraju, M. Cogswell, A. Das, R. Vedantam, D. Parikh, D. Batra, et al., Grad-cam: Visual explanations from deep networks via gradient-based localization., in: ICCV, 2017, pp. 618–626.
- [23] B. Zhou, A. Khosla, A. Lapedriza, A. Oliva, A. Torralba, Learning deep features for discriminative localization, in: Proceedings of the IEEE Conference on Computer Vision and Pattern Recognition, 2016, pp. 2921–2929.
- [24] W. Bai, O. Oktay, M. Sinclair, H. Suzuki, M. Rajchl, G. Tarroni, B. Glocker, A. King, P. M. Matthews, D. Rueckert, Semi-supervised learning for network-based cardiac mr image segmentation, in: International Conference on Medical Image Computing and Computer-Assisted Intervention, Springer, 2017, pp. 253–260.
- [25] C. Baur, S. Albarqouni, N. Navab, Semi-supervised deep learning for fully convolutional networks, in: International Conference on Medical Image Computing and Computer-Assisted Intervention, Springer, 2017, pp. 311–319.
- [26] S. Min, X. Chen, A robust deep attention network to noisy labels in semi-supervised biomedical segmentation, arXiv preprint arXiv:1807.11719.
- [27] Y. Zhou, Y. Wang, P. Tang, W. Shen, E. K. Fishman, A. L. Yuille, Semi-supervised multi-organ segmentation via multi-planar co-training, arXiv preprint arXiv:1804.02586.
- [28] C. S. Perone, P. Ballester, R. C. Barros, J. Cohen-Adad, Unsupervised domain adaptation for medical imaging segmentation with self-ensembling, arXiv preprint arXiv:1811.06042.
- [29] S. Gupta, J. Hoffman, J. Malik, Cross modal distillation for supervision transfer, in: Proceedings of the IEEE Conference on Computer Vision and Pattern Recognition, 2016, pp. 2827–2836.
- [30] I. Radosavovic, P. Dollár, R. Girshick, G. Gkioxari, K. He, Data distillation: Towards omni-supervised learning, arXiv preprint arXiv:1712.04440.

- [31] N. Souly, C. Spampinato, M. Shah, Semi supervised semantic segmentation using generative adversarial network, in: Computer Vision (ICCV), 2017 IEEE International Conference on, IEEE, 2017, pp. 5689–5697.
- [32] W.-C. Hung, Y.-H. Tsai, Y.-T. Liou, Y.-Y. Lin, M.-H. Yang, Adversarial learning for semi-supervised semantic segmentation, in: Proceedings of the British Machine Vision Conference (BMVC), 2018, p. 1.
- [33] Y. Zhang, L. Yang, J. Chen, M. Fredericksen, D. P. Hughes, D. Z. Chen, Deep adversarial networks for biomedical image segmentation utilizing unannotated images, in: International Conference on Medical Image Computing and Computer-Assisted Intervention, Springer, 2017, pp. 408–416.
- [34] P. Luc, C. Couprie, S. Chintala, J. Verbeek, Semantic segmentation using adversarial networks, arXiv preprint arXiv:1611.08408.
- [35] A. Blum, T. Mitchell, Combining labeled and unlabeled data with co-training, in: Proceedings of the eleventh annual conference on Computational learning theory, ACM, 1998, pp. 92–100.
- [36] K. Nigam, R. Ghani, Understanding the behavior of co-training, in: Proceedings of KDD-2000 workshop on text mining, Citeseer, 2000, pp. 15–17.
- [37] X. Wan, Co-training for cross-lingual sentiment classification, in: Proceedings of the Joint Conference of the 47th Annual Meeting of the ACL and the 4th International Joint Conference on Natural Language Processing of the AFNLP: Volume 1-volume 1, Association for Computational Linguistics, 2009, pp. 235–243.
- [38] B. Maeireizo, D. Litman, R. Hwa, Co-training for predicting emotions with spoken dialogue data, in: Proceedings of the ACL 2004 on Interactive poster and demonstration sessions, Association for Computational Linguistics, 2004, p. 28.
- [39] A. Levin, P. A. Viola, Y. Freund, Unsupervised improvement of visual detectors using co-training., in: ICCV, Vol. 1, 2003, pp. 626–633.

- [40] S. Qiao, W. Shen, Z. Zhang, B. Wang, A. Yuille, Deep co-training for semi-supervised image recognition, arXiv preprint arXiv:1803.05984.
- [41] D. Cooper, J. Freeman, On the asymptotic improvement in the outcome of supervised learning provided by additional nonsupervised learning, *IEEE Transactions on Computers* 19 (11) (1970) 1055–1063. doi:10.1109/T-C.1970.222832.
- [42] A. P. Dempster, N. M. Laird, D. B. Rubin, Maximum likelihood from incomplete data via the em algorithm, *JOURNAL OF THE ROYAL STATISTICAL SOCIETY, SERIES B* 39 (1) (1977) 1–38.
- [43] O. Chapelle, B. Schölkopf, A. Zien, *Semi-Supervised Learning*, 1st Edition, The MIT Press, 2010.
- [44] D. hyun Lee, Pseudo-label: The simple and efficient semi-supervised learning method for deep neural networks.
- [45] Y. Grandvalet, Y. Bengio, Entropy regularization, in: O. Chapelle, B. Schölkopf, A. Zien (Eds.), *Semi-Supervised Learning*, MIT Press, 2006, pp. 151–168.
- [46] A. Rasmus, M. Berglund, M. Honkala, H. Valpola, T. Raiko, Semi-supervised learning with ladder networks, in: C. Cortes, N. D. Lawrence, D. D. Lee, M. Sugiyama, R. Garnett (Eds.), *Advances in Neural Information Processing Systems* 28, Curran Associates, Inc., 2015, pp. 3546–3554.
- [47] D. P. Kingma, S. Mohamed, D. Jimenez Rezende, M. Welling, Semi-supervised learning with deep generative models, in: Z. Ghahramani, M. Welling, C. Cortes, N. D. Lawrence, K. Q. Weinberger (Eds.), *Advances in Neural Information Processing Systems* 27, Curran Associates, Inc., 2014, pp. 3581–3589.
- [48] S. Laine, T. Aila, Temporal ensembling for semi-supervised learning, CoRR abs/1610.02242. arXiv:1610.02242.

- [49] A. Tarvainen, H. Valpola, Weight-averaged consistency targets improve semi-supervised deep learning results, CoRR abs/1703.01780. [arXiv:1703.01780](#).
- [50] I. Goodfellow, J. Shlens, C. Szegedy, Explaining and harnessing adversarial examples, in: International Conference on Learning Representations, 2015, p. 1.
- [51] T. Miyato, S. ichi Maeda, M. Koyama, K. Nakae, S. Ishii, Distributional smoothing by virtual adversarial examples., CoRR abs/1507.00677.
- [52] A. Oliver, A. Odena, C. A. Raffel, E. D. Cubuk, I. Goodfellow, Realistic evaluation of deep semi-supervised learning algorithms, in: S. Bengio, H. Wallach, H. Larochelle, K. Grauman, N. Cesa-Bianchi, R. Garnett (Eds.), Advances in Neural Information Processing Systems 31, Curran Associates, Inc., 2018, pp. 3239–3250.
- [53] I. Goodfellow, J. Pouget-Abadie, M. Mirza, B. Xu, D. Warde-Farley, S. Ozair, A. Courville, Y. Bengio, Generative adversarial nets, in: Z. Ghahramani, M. Welling, C. Cortes, N. D. Lawrence, K. Q. Weinberger (Eds.), Advances in Neural Information Processing Systems 27, Curran Associates, Inc., 2014, pp. 2672–2680.
- [54] L. Breiman, Bagging predictors, Machine learning 24 (2) (1996) 123–140.
- [55] C. Xu, D. Tao, C. Xu, A survey on multi-view learning, arXiv preprint [arXiv:1304.5634](#).
- [56] G. Litjens, T. Kooi, B. E. Bejnordi, A. A. A. Setio, F. Ciompi, M. Ghafoorian, J. A. van der Laak, B. Van Ginneken, C. I. Sánchez, A survey on deep learning in medical image analysis, Medical image analysis 42 (2017) 60–88.
- [57] J. Dolz, C. Desrosiers, I. Ben Ayed, 3D fully convolutional networks for sub-cortical segmentation in MRI: A large-scale study, NeuroImage 170 (2018) 456–470.

- [58] J. Dolz, K. Gopinath, J. Yuan, H. Lombaert, C. Desrosiers, I. B. Ayed, Hyperdense-net: A hyper-densely connected cnn for multi-modal image segmentation, *IEEE transactions on medical imaging*.
- [59] T. Miyato, S.-i. Maeda, S. Ishii, M. Koyama, Virtual adversarial training: a regularization method for supervised and semi-supervised learning, *IEEE transactions on pattern analysis and machine intelligence*.
- [60] O. Bernard, A. Lalande, C. Zotti, F. Cervenansky, X. Yang, P. Heng, I. Cetin, K. Lekadir, O. Camara, M. A. G. Ballester, G. Sanroma, S. Napel, S. Petersen, G. Tziritas, E. Grinias, M. Khened, V. A. Kollerathu, G. Krishnamurthi, M. Roh, X. Pennec, M. Sermesant, F. Isensee, P. Jger, K. H. Maier-Hein, P. M. Full, I. Wolf, S. Engelhardt, C. F. Baumgartner, L. M. Koch, J. M. Wolterink, I. Igum, Y. Jang, Y. Hong, J. Patravali, S. Jain, O. Humbert, P. Jodoin, Deep learning techniques for automatic mri cardiac multi-structures segmentation and diagnosis: Is the problem solved?, *IEEE Transactions on Medical Imaging* 37 (11) (2018) 2514–2525. doi:10.1109/TMI.2018.2837502.
- [61] F. Prados, J. Ashburner, C. Blaiotta, T. Brosch, J. Carballido-Gamio, M. J. Cardoso, B. N. Conrad, E. Datta, G. Dávid, B. De Leener, et al., Spinal cord grey matter segmentation challenge, *Neuroimage* 152 (2017) 312–329.
- [62] O. Ronneberger, P. Fischer, T. Brox, U-net: Convolutional networks for biomedical image segmentation, in: *International Conference on Medical image computing and computer-assisted intervention*, Springer, 2015, pp. 234–241.